Nanopore size effect on critical infiltration depth of liquid nanofoam as a reusable energy absorber

Cite as: J. Appl. Phys. **125**, 044303 (2019); https://doi.org/10.1063/1.5065485
Submitted: 10 October 2018 . Accepted: 12 January 2019 . Published Online: 30 January 2019

Mingzhe Li, Lijiang Xu, and Weiyi Lu

Journal of Applied Physics ARTICLE scitation.org/journal/jap

Nanopore size effect on critical infiltration depth of liquid nanofoam as a reusable energy absorber

Cite as: J. Appl. Phys. **125**, 044303 (2019); doi: 10.1063/1.5065485
Submitted: 10 October 2018 · Accepted: 12 January 2019 ·
Published Online: 30 January 2019

Mingzhe Li, Lijiang Xu, and Weiyi Lu[a)]

AFFILIATIONS

Department of Civil and Environmental Engineering, Michigan State University, East Lansing, Michigan 48824, USA

[a)]Author to whom correspondence should be addressed: wylu@egr.msu.edu

ABSTRACT

Liquid flow in nano-environment has been utilized as an advanced mechanism of energy absorption. While the process of liquid outflow from nanopores has been shown to have a significant effect on the system's energy absorption efficiencies, its mechanism remains poorly understood. Here, we have studied the liquid defiltration behavior of liquid nanofoam (LN) systems by controlling the infiltration depth. The LN samples, composed of a different non-wettable liquid phase and hydrophobic nanoporous silica with wide pore size distribution, have been compressed in two different loading modes under the quasi-static condition, i.e., the single-step compression and consecutive-step compression. Considerably different mechanical behaviors have been observed in these two loading modes, suggesting that the liquid outflow from nanopores is determined by the critical infiltration depth D^*. The nanopore size effect on D^* is further studied by a consecutive-step cyclic test. It has been shown that D^* increases as the pore size gets smaller, which is related to gas solubility and diffusion rate in the nano-environment. The electrolyte concentration and temperature dependences of the critical infiltration depth have also been investigated. These findings provide a better understanding of the liquid outflow from nanopores and can be exploited to facilitate the design of next-generation reusable energy absorption systems.

I. INTRODUCTION

Understanding liquid motion in nano-environment is of great significance for a wide range of applications, including drug delivery, molecular transportation, catalysis, sensing, energy absorption, and many others.[1–5] Recently, a liquid nanofoam (LN) system, which employs the liquid flow in nanopores as its energy absorption mechanism, has received increasing attention.[6–11] In an LN system composed of liquid and a hydrophobic silica gel, the liquid can be driven into the nanopores when an applied external load is sufficiently high, leading to the absorption of a tremendous amount of energy. Upon removal of the external load, the liquid may or may not defiltrate from the nanopores. Although the mechanistic determinants for the liquid defiltration or the liquid outflow process remain poorly understood, it is clear that defiltration contributes to the energy absorption properties of the LN system. Sun *et al.* converted an elastic spring like LN system into an energy absorber with high efficiency by suppressing the liquid defiltration.[12]

It has been demonstrated in previous studies that the liquid defiltration behavior in the nano-environment is sensitive to the quality of surface treatment,[13,14] pore geometry,[15,16] species and concentration of electrolyte,[17] relaxation time,[18,19] degree of liquid degassing,[20] and temperature.[21] In addition to these factors, Borman *et al.* have found that the transition of a liquid from nonwetting to wetting in porous structures is related to the degree of filling, i.e., the infiltration depth, using percolation, and fluctuation theories.[22–26] For instance, as the infiltration depth reaches a critical value of 0.9, the recoverability of the system at 279 K becomes zero, i.e. no liquid outflow occurs.[22] In the current work, we have further hypothesized that the critical infiltration depth is a function of nanopore size. To test this hypothesis, we have examined the liquid outflow behavior in nanopores using a nanoporous silica gel with a wide pore size distribution. Our results show that the critical infiltration depth increases as the nanopore size becomes smaller.

II. METHODS

The nanoporous material used in the current study was hydrophobic precipitated silica (Perform-O-Sil 668,

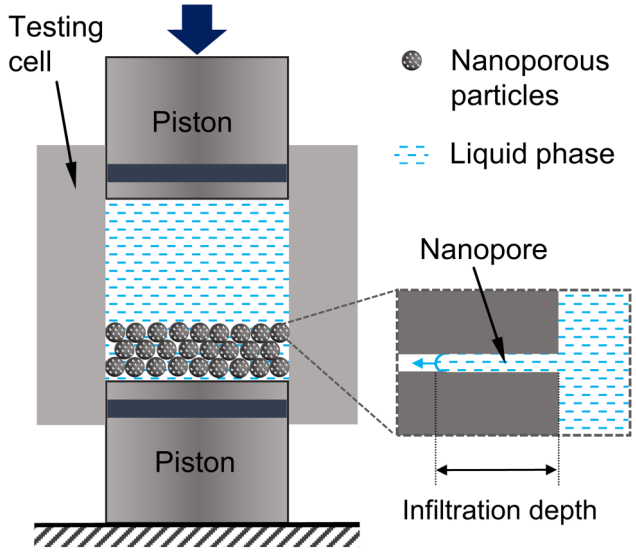

FIG. 1. Schematic of the experimental setup.

Nottingham Corp.). The as-received material was in powder form, with the average particle size around 4 μm. Due to the low strength of the porous frame (lower than the required activation pressure for mercury porosimetry analysis method) and the relatively large nanopores (>100 nm, the upper limit of gas adsorption analysis method), mercury porosimetry and Brunauer–Emmett–Teller (BET) methods were not applicable for analyzing the porous structure of this nanoporous silica. Instead, water porosimetry[27–29] was used to characterize the porous structure. The specific nanopore volume of the nanoporous silica was measured to be 1.8 cm^3/g. The porosity was then calculated as 80% based on the measured specific nanopore volume and the density of solid silica.

A cylindrical testing cell and two pistons (Fig. 1) made of poly(methyl methacrylate) were designed to investigate the nanoscale liquid motion of the LN. The cross-sectional area of the pistons, A_p, was 286 mm^2. The pistons were equipped with O-rings to seal the LN sample which contained 0.3 g of the nanoporous silica gel and 2 g of liquid. The nanoporous silica gel was pre-compressed into a close packed disk to minimize the air trapped in between the particles. The liquid phase used in the current study was de-ionized (DI) water, 23 wt. % lithium chloride (LiCl) aqueous solution, and 46 wt. % LiCl aqueous solution.

The LN samples were compressed by an Instron 5982 universal tester equipped with an environmental chamber (Instron, Inc.) at 20 °C, 50 °C, and 80 °C. High vacuum grease was applied on the O-rings to reduce the friction between the O-rings and pistons. No liquid leakage was observed during all compression tests. The applied pressure was calculated as $P = F/A_p$, where F is the force exerted on the piston. For the single-step test, the applied force increased gradually to 2 kN, which was equivalent to an applied pressure of 7 MPa, at a constant loading rate of 2 mm/min, after which the crosshead of the Instron machine was moved back at the same speed. The loading-unloading process was repeated for five cycles. For the consecutive-step test, an LN sample with identical solid and liquid content was compressed at six consecutive steps at the same loading rate. The peak pressure of each step was increased monotonically from 1.25 MPa to 7 MPa. To study the liquid defiltration behavior of each step, the LN sample was compressed for three cycles in each step. The specific volume change of the LN sample was defined as $\Delta V = A_p\delta_p/m$, where δ_p and m are the piston displacement and the mass of the nanoporous silica gel, respectively.

III. RESULTS AND DISCUSSION

In the single-step test, the applied force increased gradually at a constant loading speed of 2 mm/min. When the pressure reached 7 MPa, the crosshead of the Instron machine was moved back at the same rate. The results of the single-step test are shown in Fig. 2. As all the subsequent cycles are nearly identical to the second one, only the first

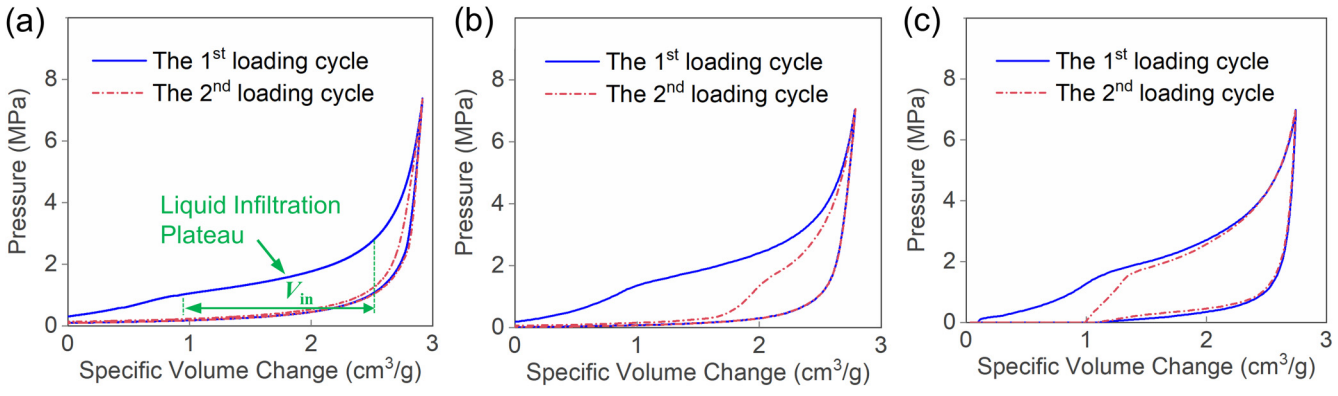

FIG. 2. Typical sorption isotherm curves of single-step test at 20 °C. Liquid phase: (a) water, (b) 23 wt. % LiCl aqueous solution, and (c) 46 wt. % LiCl aqueous solution.

two loading-unloading curves are shown here for clarity. For water based-LN, a non-linear pressure-volume change is observed in the first loading cycle [Fig. 2(a)]. Microscopically, forced liquid molecules flow into the nanopores starting at 1.0 MPa associated with the specific volume change in the LN of 0.9 cm^3/g and ends up at the point of 3.0 MPa and 2.7 cm^3/g. This process is referred to as liquid infiltration and identified as the stress plateau of the loading curve.[6,9] For self-comparison purposes, the starting point of the infiltration plateau is defined as the point at which the slope of the loading curve is reduced by 50% of that of the initial elastic region and the ending point is defined as the point at which the slope increases by 50% of that of the infiltration plateau. The infiltration pressure (P_{in}) of the LN is the critical pressure forcing the liquid molecules into the nanopores, which is a function of the nanopore size based on the classic Laplace-Young equation.[30] The infiltration volume (V_{in}) of the LN, which is determined by the width of the infiltration plateau, is around 1.8 cm^3/g. In the single-step test, this value is the same as the total pore volume of the nanoporous silica gel characterized by the water porosimetry method. In the second loading cycle, the curve is no longer hysteretic indicating that nearly zero liquid defiltration takes place in the unloading process of the first cycle. The energy absorption behavior of the LN is similar to the plastic behavior of regular foams which is permanent. As the liquid phase changes to 23 wt. % LiCl aqueous solution, the initial P_{in} increases to 1.5 MPa due to the increased effective surface tension of the liquid phase.[31] More importantly, the reusability of LN increases to approximately 25%, i.e., 25% liquid molecules defiltrate from the nanopore during the unloading process of the first cycle. The reusability is further promoted to 80% when the concentration of LiCl solution increases to 46 wt. %.

The considerably different liquid defiltration behavior is likely to result from the gas-liquid interaction in the nanopores.[32] For water based-LN, as the external loading reaches P_{in} and increases, the liquid gradually enters the nanopores, leading to an increasing infiltration depth (inset in Fig. 1). The normalized infiltration depth D is defined as $D = V_l/V_p$, where V_l and V_p are the volume of intruded liquid molecules and total available pore volume of the nanoporous material, respectively. As D increases, the gas phase in the nanopores is compressed and stores more potential energy. Consequently, the effective gas solubility in the confined liquid molecules is significantly enhanced.[33] Note that due to the entrapment, the gas solubility in nano-environment is distinct from that in the bulk phase.[34] Once a critical value D^* is reached, the effective gas solubility in the confined liquid molecules is sufficiently high and the gas can quickly diffuse into the bulk liquid phase. After removal of the external loading, the gas phase, which can act as the driving force for liquid defiltration, is absent.[35] Thus, no liquid outflow can be observed as the liquid-solid interfacial tension is not sufficient. As the LiCl concentration increases, the gas solubility is remarkably reduced.[36,37] Therefore, for LiCl solution based-LN samples, the gas phase is highly compressed and stores higher potential energy in the nanopores in the infiltration process. During unloading, the stored potential energy in the gas phase is released. Combining with the liquid-solid interfacial tension, the driving force is high enough to promote the liquid outflow. The gas diffusion process is validated by the air bubbles generated in the bulk liquid phase after the single-step compressive tests (Fig. 3). Before the test, the nanoporous silica particles are a close-packed layer with no visible air bubbles [Fig. 3(a)]. For water based-LN, the volume of the silica gel layer expands dramatically during the unloading process, with a large amount of visible air bubbles in the testing cell [Fig. 3(b)]. The air, initially trapped in the nanopores, diffuses out of nanopores, and the nanopore volume is occupied by infiltrated liquid molecules. In this single-step compression

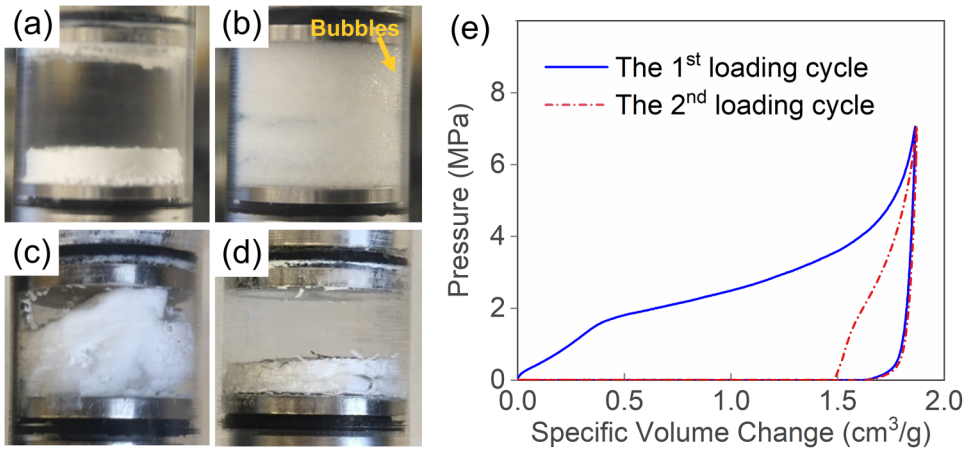

FIG. 3. (a)–(d) Snapshots of the LN sample: (a) before single-step test; (b)–(d) after single-step test. Liquid phase: (b) water, (c) 23 wt. % LiCl aqueous solution, and (d) 46 wt. % LiCl aqueous solution. (e) Typical sorption isotherm curves of degassed 46 wt. % LiCl aqueous solution based-LN.

test, as all the nanopores are completely filled by the liquid molecules, the D* is reached. For LN with 23 wt. % LiCl aqueous solution, the volume expansion of the silica gel layer after the first loading cycle is smaller than that of water based-LN, indicating that less gas phase diffuses out of the nanopores. The non-diffused gas phase performs as the driving force for liquid outflow. Thus, the LN sample shows 25% reusability. For LN with 46 wt. % LiCl aqueous solution, the volume of the silica gel layer almost remains the same after completion of the first loading cycle, which indicates that most of the gas phase stays in the nanopores. As a result, nearly 80% of liquid molecules defiltrate from the nanopores.

The single-step compression test on degassed LN samples further validates that the gas phase in the nanopores acts as the dominant driving force during the liquid defiltration process. The degassed LN sample was prepared by placing the mixture in vacuum (4 kPa) for 24 h. Thus, both the gas dissolved in liquid and small bubbles in the mixture were almost entirely eliminated, while the gas in nanopores was only partially removed.[20] Upon compression, the remaining gas phase in the nanopores was more prone to be dissolved in the liquid and the driving force for liquid outflow was much reduced compared with the LN without degassing. The infiltration width of the second loading cycle of 46 wt. % LiCl aqueous solution based-LN was reduced from 80% [Fig. 2(c)] to 15% [Fig. 3(e)]. For water and 26 wt. % LiCl aqueous solution based-LNs, the extent of liquid outflow became nearly zero (Fig. S1 in the supplementary material). These results confirm that the gas phase is the primary driving force for the liquid outflow. Please also note that the pressure level of the plateau in the unloading curve in Fig. 3(e) (~0.1 MPa) is much lower than that in Fig. 2(c) (~0.8 MPa). This reduced pressure indicates that part of the driving force for liquid outflow, i.e., the gas phase, is lost.

The above experimental results are contradictory to the literature results,[20] in which the liquid outflow is promoted by degassing. This is attributed to the pore size effect on liquid outflow in these two LN systems. In the ZSM-5 zeolite based-LN,[20] the pore size is ~2 nm and the liquid outflow path can be easily blocked by the excessive gas phase. Therefore, by removing the excessive gas, the liquid outflow path becomes continuous, which benefits liquid outflow. Besides, due to the ultra-small pore size, the LN has a relatively high P_{in} (~18 MPa) and the corresponding defiltration pressure is high enough to drive the liquid out. Therefore, the gaseous driving force can be neglected. While in the current system, the pore size is 1 or 2 orders of magnitude larger and the gas blocking effect can be ignored. In addition, P_{in} (~2 MPa) is relatively low and the corresponding defiltration pressure is insufficient for liquid outflow; thus, the gaseous driving force becomes dominant. Consequently, degassing leads to a lower liquid outflow extent in the current LN system.

To study the effect of nanopore size on D*, we have characterized the nanoporous structure of the silica gel by the water porosimetry method. Following the classic Laplace-Young equation, $r = 2\gamma/P_{in}$ (where γ is the excessive solid-liquid interfacial tension with a value of 72.8 mN/m[29] and r is the effective nanopore radius). The pressure-volume change curve is converted into nanopore size distribution by the water porosimetry analysis. The nanopores of the silica gel used in the current study exhibit a wide diameter distribution from 40 nm to 400 nm [Fig. 4(a)]. The pore size distribution characterized by water porosimetry is further verified from the SEM photos of the silica gel as shown in Fig. 4(b). Combining the pore size distribution and the consecutive loading mode, we reveal the effect of nanopore size on D*.

In the consecutive-step test, the LN was compressed at six consecutive steps at a constant loading rate of 2 mm/min. The peak pressure of each step was increased monotonically from 1.25 MPa to 7 MPa. Thus, the widely distributed nanopores are divided into six segments with different average nanopore sizes by controlling the applied peak pressure. The combination of all the test curves matches well with the

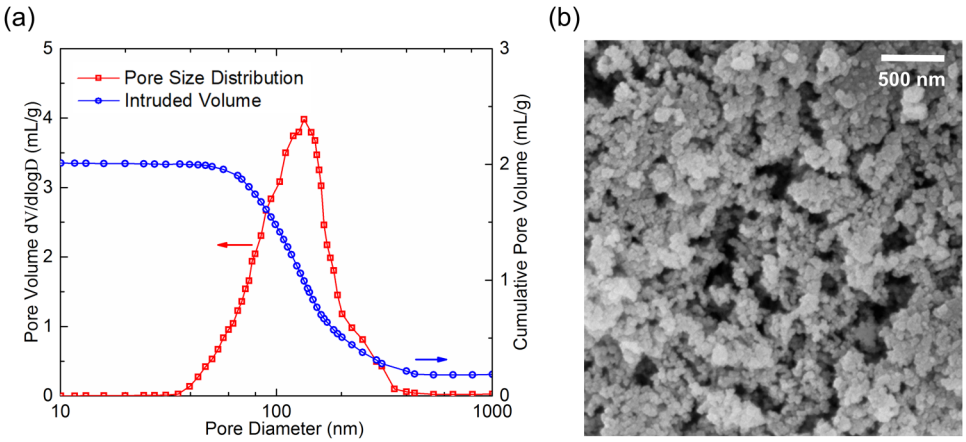

FIG. 4. (a) Pore size distribution of silica gel and intruded volume vs. pore size curve. (b) Typical SEM image of the nanoporous silica.

loading-unloading curve of the single-step test (Fig. 5), indicating that all the nanopores in the silica gel are involved in the stepwise tests. More importantly, for water based-LN, all the sorption isotherm curves of the six steps show partial repeatability of the liquid infiltration process as indicated by the overlapped areas between steps [Fig. 5(a)], which is not shown in the single-step test [Fig. 2(a)]. The repeatable hysteretic behavior demonstrates that the energy absorption mechanism of LN is associated with the liquid motion in nanopores rather than the plastic deformation such as the buckling of the nanopore walls which is irreversible. The repeatable liquid infiltration process also indicates that part of the liquid molecules outflow from the nanopores when the external pressure is removed. In other words, by controlling the peak pressure, the D^* is not reached in each step. Similarly, the reusability of LN is promoted in the consecutive-step test for LN with LiCl aqueous solution [Figs. 5(b) and 5(c)], indicating that more liquid molecules defiltrate from the nanopores in the consecutive-step test than in the single-step test.

To better understand the effect of nanopore size on D^*, the loading cycle is repeated three times for each step [Fig. 5(d)]. The loading cycles are referred to as $L_{i,j}$, where i is the step number and j is the cycle number in each step. D^* can be determined from the recoverability after the first loading cycle in each step (see details in the supplementary material). Figure 6(a) shows the relationship between D^* and r_i of LN containing various aqueous solutions at 20 °C. Note for smaller pores, D^* is still underestimated here. As the loading increases, the larger pores are first filled while the smaller ones are empty. As the liquid molecules are forced to enter smaller pores, the larger ones have been already fully filled. Thus, liquid molecules in smaller pores will interact with neighboring larger pores, which is known as "multi-particle interaction."[25] This multi-particle interaction leads to a reduced D^* for smaller pores in this study. As shown in Fig. 6(a), for water based-LN, D^* increases from 0.75 to 0.83 as the pore size decreases from 150 nm to 70 nm. The trend is consistent with the literature results,[22] in which Borman *et al.* observed $D^* = 0.9$ for an LN system composed of water and a hydrophobic silica gel with an average pore size of 13 nm. As the concentration of LiCl increases, D^* also increases. As previously validated in the single-step tests, this is due to the reduced gas solubility in the liquid phase with higher

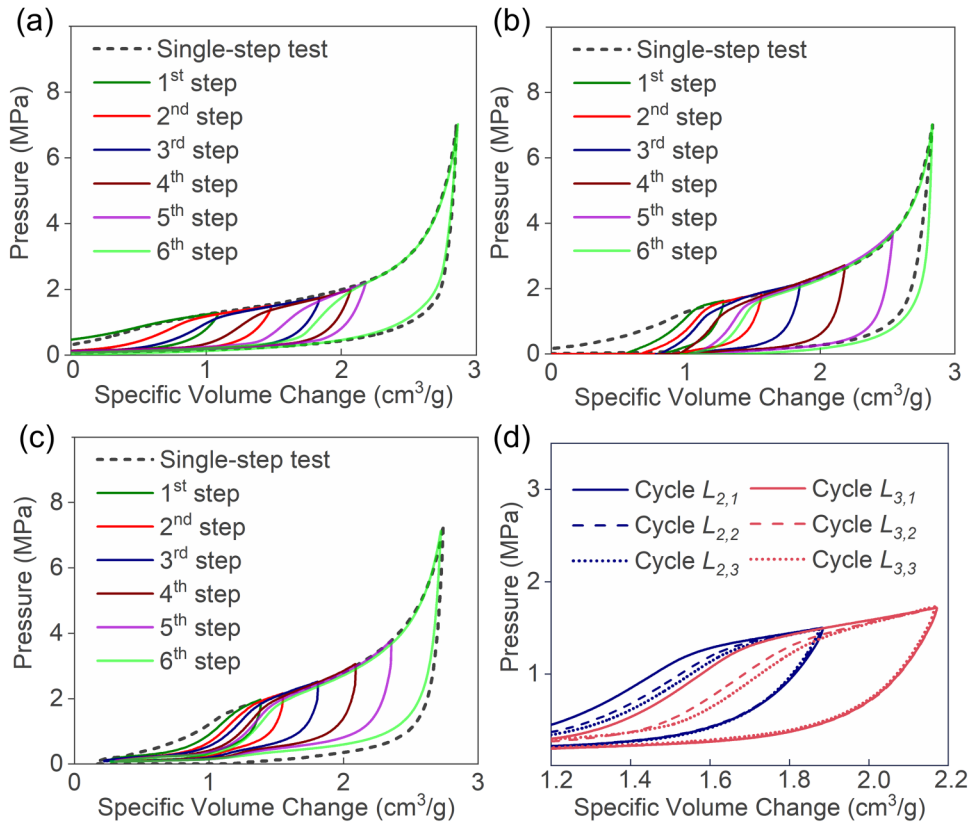

FIG. 5. (a)–(c) Typical sorption isotherm curves of the consecutive-step test at 20 °C. Liquid phase: (a) water, (b) 23 wt. % LiCl aqueous solution, and (c) 46 wt. % LiCl aqueous solution. (d) Typical sorption isotherm curves of the 2nd and 3rd steps in the consecutive-step cyclic test of water-based LN.

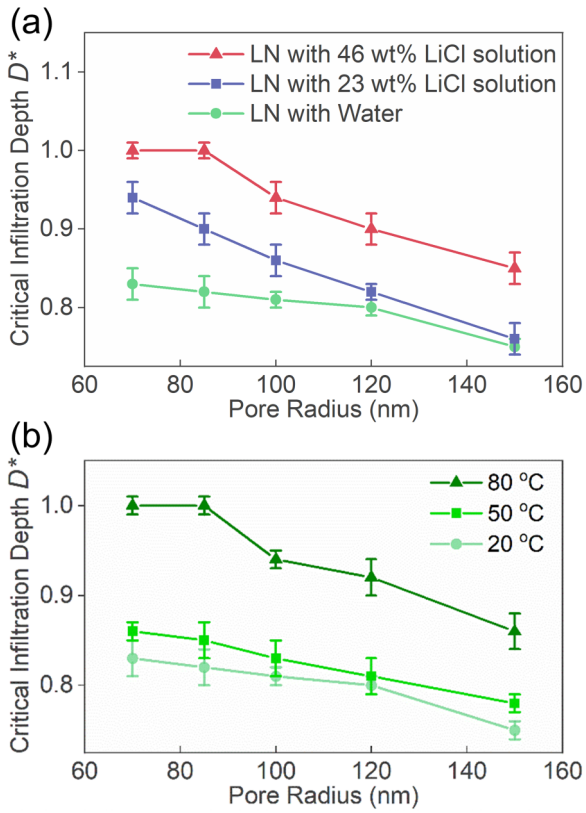

FIG. 6. Relationship between critical infiltration depth D^* and pore radius r_j. (a) LN containing various aqueous solutions at 20 °C; (b) water based LN at different temperatures.

electrolyte concentration.[36,37] The gas phase tends to be sealed in the nanopore and drives liquid defiltration, leading to a larger D^*.

Figure 6(a) also shows that D^* increases as the pore size gets smaller, i.e., it is easier for liquid molecules to defiltrate from smaller pores than from larger ones at the same infiltration depth. The pore size effect on D^* is associated with the gas-liquid interaction in nanopores. (1) As the pore size decreases, the solvation of the gas phase in the confined liquid phase becomes more difficult.[33] In larger pores, the gas molecules can be quickly dissolved in the liquid. However, the water molecules cannot surround and dissolve the gas molecules due to insufficient space in smaller pores, leading to the formation of gas clusters. Therefore, it promotes the retention of the "driving force" for defiltration in smaller pores. (2) It is easier for smaller pores to regain the "driving force" if the gas molecules were dissolved in the liquid phase during the loading process. Upon unloading, in smaller pores, the dissolved gas molecules can diffuse back, nucleate, and grow in the "sealed end" of the nanopores rather than directly diffuse into the bulk liquid phase, which promotes the liquid outflow as well.[32] With these two synergetic mechanisms, the value of D^* in smaller nanopores is much larger than that in larger nanopores. Please note that the gas phase effect on liquid outflow can be quantified by measuring the gas pressure in the nanopore during liquid infiltration. However, due to the dynamic gas diffusion process during liquid infiltration, the infiltration pressure or the infiltration depth cannot be directly converted to the gas pressure by ideal gas law.

Figure 6(b) shows that D^* is sensitive to temperature change. D^* increases at elevated temperature, which suggests that the increased temperature promotes the liquid outflow. This finding is in agreement with previous works.[38,39] The thermal effect on liquid defiltration is attributed to the temperature sensitive defiltration pressure.[40]

IV. CONCLUSIONS

In summary, the liquid defiltration behavior of the LN is experimentally investigated. The system reusability under two different loading modes is distinct from each other. The degree of liquid defiltration is a function of the nanopore size. When the nanopore size decreases, both D^* and the degree of liquid defiltration increase. This is related to the reduction of gas solubility and diffusion rate in the nano-environment. The smaller the nanopore is, the larger tolerance the system has. With the enhanced D^*, the LN can be implemented for cyclic loading applications as a reusable energy absorber.

SUPPLEMENTARY MATERIAL

In the supplementary material, the results of the single-step test on degassed LN, high-pressure holding test, consecutive-step cyclic test, the details on the determination of critical infiltration depth D^*, and the measurement of characteristic time of liquid outflow are included.

ACKNOWLEDGMENTS

This study was financially supported by the National Science Foundation (NSF) (No. CBET-1803695) and the Michigan State University Startup grant.

REFERENCES

[1]A. Bianco, K. Kostarelos, and M. Prato, Curr. Opin. Chem. Biol. **9**, 674 (2005).
[2]P. Chen, J. Gu, E. Brandin, Y. R. Kim, Q. Wang, and D. Branton, Nano Lett. **4**, 2293 (2004).
[3]D. Vairavapandian, P. Vichchulada, and M. D. Lay, Anal. Chim. Acta **626**, 119 (2008).
[4]A. A. Gusev and O. Guseva, Adv. Mater. **19**, 2672 (2007).
[5]V. Eroshenko, R. C. Regis, M. Soulard, and J. Patarin, J. Am. Chem. Soc. **33**, 8129 (2001).
[6]L. Liu, X. Chen, W. Lu, A. Han, and Y. Qiao, Phys. Rev. Lett. **102**, 184501 (2009).
[7]S. H. Ganjiani and A. Hossein Nezhad, J. Phys. Chem. C **120**, 11864 (2016).
[8]H. Liu and G. Cao, J. Phys. Chem. C **120**, 5213 (2016).
[9]M. Li and W. Lu, Phys. Chem. Chem. Phys. **19**, 17167 (2017).
[10]M. Li and W. Lu, AIP Adv. **7**, 055312 (2017).
[11]M. Li, J. Li, S. Barbat, R. Baccouche, and W. Lu, Compos. Struct. **200**, 120 (2018).

[12]Y. Sun, W. Lu, and Y. Li, Appl. Phys. Lett. **105**, 121609 (2014).
[13]A. Han and Y. Qiao, Chem. Eng. J. **141**, 379 (2008).
[14]A. Han and Y. Qiao, Chem. Phys. Lett. **454**, 294 (2008).
[15]S. P. Rigby and K. J. Edler, J. Colloid Interface Sci. **250**, 175 (2002).
[16]T. Kim, A. Han, and Y. Qiao, J. Appl. Phys. **104**, 034304 (2008).
[17]F. B. Surani and Y. Qiao, J. Appl. Phys. **100**, 034311 (2006).
[18]V. D. Borman, A. A. Belogorlov, and V. N. Tronin, Phys. Rev. E **93**, 1 (2016).
[19]V. D. Borman, A. A. Belogorlov, and V. N. Tronin, Colloids Surf. A Physicochem. Eng. Asp. **496**, 63 (2016).
[20]Y. Zhang, R. Luo, Q. Zhou, X. Chen, and Y. Dou, Appl. Sci. **8**, 1065 (2018).
[21]Y. T. Sun, J. Xu, Y. B. Li, X. Q. Xu, C. Liu, and X. Chen, J. Nanomater. **2013**, 249369 (2013).
[22]V. D. Borman, A. A. Belogorlov, V. A. Byrkin, V. N. Tronin, and V. I. Troyan, JETP Lett. **95**, 511 (2012).
[23]V. D. Borman, A. A. Belogorlov, V. A. Byrkin, V. N. Tronin, and V. I. Troyan, J. Exp. Theor. Phys. **117**, 1139 (2013).
[24]V. D. Borman, A. A. Belogorlov, A. M. Grekhov, and V. N. Tronin, Phys. Lett. A **378**, 2888 (2014).
[25]V. D. Borman, A. A. Belogorlov, V. M. Zhuromskii, and V. N. Tronin, J. Exp. Theor. Phys. **121**, 1027 (2015).
[26]V. D. Borman, V. N. Tronin, and V. A. Byrkin, Phys. Lett. A **380**, 1615 (2016).
[27]J. Rouquerol, G. V. Baron, R. Denoyel, H. Giesche, J. Groen, P. Klobes, P. Levitz, A. V. Neimark, S. Rigby, R. Skudas, K. Sing, M. Thommes, and K. Unger, Microporous Mesoporous Mater. **154**, 2 (2012).
[28]L. Andersson, P. T. Larsson, L. Wågberg, and L. Bergström, J. Am. Ceram. Soc. **96**, 1916 (2013).
[29]A. Fadeev and V. Eroshenko, J. Colloid Interface Sci. **187**, 275 (1997).
[30]Y. Qiao, L. Liu, and X. Chen, Nano Lett. **9**, 984 (2009).
[31]A. Han, X. Chen, and Y. Qiao, Langmuir **24**, 7044 (2008).
[32]A. Han, X. Kong, and Y. Qiao, J. Appl. Phys. **100**, 014308 (2006).
[33]Y. Qiao, G. Cao, and X. Chen, J. Am. Chem. Soc., 2355 (2007).
[34]A. Luzar and D. Bratko, J. Phys. Chem. B **109**, 22545 (2005).
[35]Y. Sun, P. Li, Y. Qiao, and Y. Li, Sci. Rep. **4**, 6547 (2014).
[36]Z. Duan and R. Sun, Chem. Geol. **193**, 257 (2003).
[37]X. Shi and S. Mao, Chem. Geol. **463**, 12 (2017).
[38]X. Kong and Y. Qiao, Philos. Mag. Lett. **85**, 331 (2005).
[39]Y. Zhang, N. Li, R. Luo, Y. Zhang, Q. Zhou, and X. Chen, J. Phys. D Appl. Phys. **49**, 025303 (2016).
[40]Y. Grosu, O. Ievtushenko, V. Eroshenko, J. M. Nedelec, and J. P. E. Grolier, Colloids Surf. A Physicochem. Eng. Asp. **441**, 549 (2014).